POLITECNICO DI TORINO
Repository ISTITUZIONALE

Surface modification of silicate, borosilicate, and phosphate bioactive glasses to improve/control protein adsorption: PART II

Original
Surface modification of silicate, borosilicate, and phosphate bioactive glasses to improve/control protein adsorption: PART II / Gobbo, V.A., Turkki, P., Santos Dias Palma, C., Parihar, V.S., Verne', E., Spriano, S., Sanches Ribeiro, A., Hytonen, V.P., Massera, J.. - In: CERAMICS INTERNATIONAL. - ISSN 0272-8842. - ELETTRONICO. - 49:8(2023), pp. 12856-12865. [10.1016/j.ceramint.2022.12.157]

Availability:
This version is available at: 11583/2979835 since: 2023-07-04T13:03:41Z

Publisher:
Elsevier Ltd

Published
DOI:10.1016/j.ceramint.2022.12.157

Terms of use:

This article is made available under terms and conditions as specified in the corresponding bibliographic description in the repository

Publisher copyright

(Article begins on next page)

18 June 2026

Ceramics International 49 (2023) 12856–12865

Contents lists available at ScienceDirect

Ceramics International

journal homepage: www.elsevier.com/locate/ceramint

Surface modification of silicate, borosilicate, and phosphate bioactive glasses to improve/control protein adsorption: PART II

Virginia Alessandra Gobbo [a,*], Paula Turkki [a,b], Cristina Santos Dias Palma [a], Vijay Singh Parihar [a], Enrica Vernè [c], Silvia Spriano [c], Andre Sanches Ribeiro [a], Vesa P. Hytönen [a,b], Jonathan Massera [a]

[a] Faculty of Medicine and Health Technology, Tampere University, 33720, Tampere, Finland
[b] Fimlab Laboratories, Biokatu 4, 33520, Tampere, Finland
[c] Department of Applied Science and Technology, Politecnico di Torino, 10129, Torino, Italy

A B S T R A C T

Bioactive glasses (BGs) are characterized by high biocompatibility and bioactivity and are particularly promising for bone tissue regeneration. Once implanted, the BGs interact with the environment and adsorb chemical moieties and biomolecules. Proteins in body fluids are critical for the success of implants, because the adsorption of specific proteins can either promote or inhibit the adhesion of surrounding tissue or other factors such as bacteria. Controlling protein adsorption by tailoring the surface properties of implanted biomaterials is fundamental. This can determine the fate of the implant. In the current study, four BG compositions (two silicates, one borosilicate, and one phosphate glass) and three model proteins (fibronectin, chimeric avidin, and streptavidin) were considered. Each BG was surface pretreated, and the adsorption of fluorescently labeled fibronectin, chimeric avidin, or streptavidin was monitored. Untreated surfaces were used as controls. The amount and spatial distribution of each protein were estimated by confocal microscopy in fluorescence modality, followed by protein clustering analysis. Although streptavidin was not adsorbed efficiently on any of the considered substrates, BGs were successfully coated with fibronectin and chimeric avidin. Both proteins showed different affinities and surface distributions as functions of the implemented pretreatment on each substrate.

1. Introduction

Bioactive glasses (BGs) are a recent class of biomaterials with interesting features such as biocompatibility, bioactivity, and osteoconductivity/osteoinductivity. BGs are particularly promising for application in bone tissue regeneration. Their highly tailorable composition allows for a wide range of physicochemical and therapeutic properties according to the intended purpose [1–3]. Furthermore, owing to their intrinsic reactivity, BGs can be superficially treated to promote the adsorption of biological moieties that are beneficial for the success of implants [4,5]. Proteins are of particular interest because they are involved in the first step of the reaction between a living tissue and an implanted BG [6]. This is crucial because it determines the fate of the device implanted in the human body [7–9]. The bulk and surface properties of a material can either promote or limit the adsorption of specific proteins. This affects the subsequent adhesion of body cells, with the recruited types changing with the adsorbed proteins or bacteria. The type of recruited cells can be also influenced by the previously adsorbed proteins [10–12]. Overall, this process determines the success of implants in the short and/or long term [7,11,12]. A better understanding of protein adsorption mechanisms will assist in the development of smart surfaces for recruiting targeted proteins. Consequently, this would promote the adhesion of the desired cells to achieve optimal and efficient tissue regeneration. Despite lacking full understanding of these phenomena, whose study started recently, some experiments have been performed to measure the affinity between the biomaterials for musculoskeletal applications and peptides/proteins of interest [11]. Fibronectin, bone sialoprotein, and bone morphogenetic proteins have been attached to titanium surfaces, with promising results. They exploited chemical-based methods such as physisorption [13], covalent grafting [13,14], crosslinking [15], electrochemical deposition [16], mechanical methods such as acid etching [13], and physical methods such as plasma treatments [13,17]. Indeed, mechanical and physical methods increase the surface-to-volume ratio and consequently increase the available area for protein adsorption [13,17]. BGs are considered to be suitable substrates for protein adsorption. Protein adsorption has been investigated both as a pretreatment for enhancing the *in vivo* response and for mimicking the *in vivo* process of protein-biomaterial interaction. Albumin and methemoglobin were adsorbed on surface-modified BG 45S5. 45S5, often referred to as Bioglass®, was the

* Corresponding author.
E-mail address: virginiaalessandra.gobbo@tuni.fi (V.A. Gobbo).

https://doi.org/10.1016/j.ceramint.2022.12.157
Received 18 August 2022; Received in revised form 1 December 2022; Accepted 15 December 2022
Available online 16 December 2022
0272-8842/© 2022 The Authors. Published by Elsevier Ltd. This is an open access article under the CC BY license (http://creativecommons.org/licenses/by/4.0/).

first bioactive glass developed by L. L. Hench in 1969 with a composition of $45SiO_2$-$6P_2O_5$-24.5CaO-24.5Na_2O in wt%. Soaking in buffer solutions or grafting glutaraldehyde improved the interaction between the protein and substrate [18,19]. In addition, fibronectin has been adsorbed on silicate and phosphate glasses (by washing the substrate at different pH and successively grafting aminosilane molecules). It was found that the surface physicochemical properties of the BGs and their chemical compositions were influential [20]. Furthermore, fibronectin-coated surfaces promote biocompatibility and cell activity [21]. Notably, a recent study investigated nonspecific protein adsorption by soaking different BG compositions in human blood serum. The authors evaluated the adsorption of 289 distinct proteins on the surfaces of interest to simulate and characterize the phenomena occurring after BG implantation in the human body [22]. Given these promising results, further studies are required to confirm the outcomes and deepen our understanding of the dynamics of protein adsorption on BGs. Our recent study evaluated the impact of various treatments on the physicochemical properties of the surfaces of four BGs (two silicates, one borosilicate, and one phosphate glass). The treatments involved soaking these BGs in either tris (hydroxymethyl)aminomethane (TRIS) or simulated body fluid (SBF) solutions and grafting with either 3-aminopropyltriethoxysilane (APTES) or quaternized APTES (Q-APTES). Wettability, surface charge, and surface chemistry can be tailored by treatment [23].

Here, we expand research on the influence of the physicochemical properties of BGs on protein adsorption. Three model proteins (fibronectin, chimeric avidin, and streptavidin) were adsorbed by four different BGs before and after surface treatment. Model proteins were selected owing to their chemical characteristics and potential roles in future applications. Fibronectin is commonly used in BG studies, as it is a ubiquitous extracellular matrix protein that is crucial in wound healing and tissue repair. It is also a prominent attachment factor for cells, and generally improves the biocompatibility of BGs. For these reasons, fibronectin is of interest both to mimic and study the biological response and to pre-coat the surface before implantation to enhance the biological response itself [20,21]. However, fibronectin has a complicated structure and multiple biological functions (Fig. 1). Meanwhile, chimeric avidin has a high affinity for the small ligand biotin, which has been used in a range of biotechnological applications. Avidins are relatively small homotetrameric proteins (Fig. 1). Finally, avidin and biotin form a strong bond that can be used to further functionalize avidin-coated BGs with biotinylated therapeutic small molecules or with a mixture of different attachments or growth factors, expanding the usability of BGs [24–26]. Furthermore, avidins exhibit antibacterial properties [27]. The aim of the current study was to assess which surface is more suitable for the adsorption of the three model proteins.

2. Materials and methods

2.1. Bioactive glasses (BGs)

Four BG compositions were produced using the melt quench method (S53P4, B25, SCNB, PhGlass). Their nominal compositions, expressed in molar percentages (mol %), are listed in Table 1.

Belgian quartz sand (SiO_2), ($CaHPO_4$) $2H_2O$, H_3BO_3, Na_2CO_3 and $CaCO_3$ were used as precursors for the silicate and borosilicate glass preparation. Belgian quartz sand (SiO_2), $Ca(PO_3)_2$, NH_6PO_4, $(NaPO_3)_6$, $SrCO_3$, and MgO were used for the phosphate glass. The protocol for producing $Ca(PO_3)_2$ is described in [20]. All the precursors were weighed and mixed in an alumina mortar. Silicate and borosilicate glasses were melted in a platinum crucible, while phosphate glass was melted in a silica crucible, as described in [23].

Midway through the melting point, the melts were mixed to ensure high homogeneity. The melts were cast into a graphite cylindrical mold (Ø = 10 mm), previously preheated at 360 °C, and annealed. The rods were cut into 2 mm thick discs and polished with silicon carbide (SiC) sandpaper (#320, #500, #800, #1200, #2500, #4000). The samples were stored at room temperature (around (24 ± 2) °C) in a desiccator.

Four pre-treatments were implemented on each substrate: soaking in (i) 0.05 M tris(hydroxymethyl)aminomethane (TRIS) buffer solution, or (ii) simulated body fluid (SBF), and silanization by grafting either (iii) 3-aminopropyltriethoxysilane (APTES) or (iv) quaternized APTES (Q-APTES). Q-APTES was synthesized as described previously [23]. Briefly, 5 ml of APTES (99%, Sigma-Aldrich) and 50 ml of dry chloroform (≥99.8%, Honeywell) were poured into a sealed tube, and 10 ml of 1-hexylbromide (98%, Sigma-Aldrich) was added under an inert atmosphere. The reaction, having place at 50 °C for 24 h monitored by thin-layer chromatography (TLC) for its proper tracking. The solvent was then removed using a rotary evaporator (55 °C, 185 rpm), affording a yellowish crude product. The crude product was purified by multiple washes with chloroform and ethyl acetate, dispersed in chloroform, sonicated for 5 min, and then filtered. This procedure was repeated 3 times in chloroform and successively in ethyl acetate (Merck KGaA, ethyl acetate). The pure product was finally maximum dried in a rotary

Table 1
BG nominal composition (mol %).

	SiO_2	P_2O_5	B_2O_3	Na_2O	CaO	SrO	MgO
S53P4	53.85	1.72	–	22.66	21.77	–	–
B25	40.39	1.72	13.46	22.66	21.77	–	–
SCNB	55.60	–	–	22.70	21.70	–	–
PhGlass	2.50	45.00	2.50	10.00	20.00	10.00	10.00

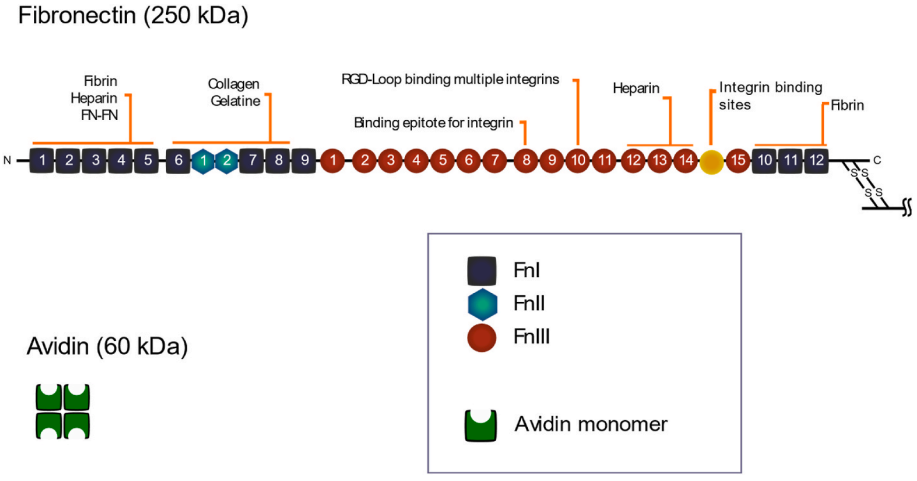

Fig. 1. Schematic molecular structure of fibronectin and chimeric avidin/streptavidin. Fibronectin is dimeric protein, where monomers (~250 kDa each) are linked with C-terminal disulphides. Chimeric avidin and streptavidin are structurally analogous homotetrameric proteins, each monomer having a binding site for biotin. The variable region in fibronectin is indicated by yellow sphere. (For interpretation of the references to color in this figure legend, the reader is referred to the Web version of this article).

evaporator for 2 h under vacuum (55 °C, 185 rpm) and in a vacuum oven overnight at 37 °C. The Q-APTES solution for pre-treating BGs was prepared by dissolving 70 mg of the final product overnight in 150 ml of ethanol (96% vol., VWR) under stirring (50 °C, 400 rpm).

TRIS buffer solution (0.05 M) was prepared by dissolving 1.66 g Trizma® Base (Trizma® Base, Primary standard and buffer, ≥99.9% (titration), crystalline, Sigma Aldrich) and 5.72 g of Trizma® HCl (Trizma® hydrochloride, reagent grade, ≥99.9% (titration), crystalline, Sigma Aldrich) in 1 L of distilled water. The solution was then stabilized for 3 h at 37 °C in a hot bath to ensure a pH value of 7.40 ± 0.02 at (37.0 ± 0.2) °C. SBF was prepared according to Kokubo's protocol, as reported in [28]. The final pH (7.40 ± 0.01) at (36.5 ± 0.1) °C was imposed by dissolving 6.118 g Trizma® Base and buffering the solution with 1 M HCl. Both solutions were stored at 4 °C and utilized within one month.

TRIS and SBF treatments were implemented by soaking each BG sample in 50 ml of the respective solutions and incubating for 72 h at 37 °C. Subsequently, the discs were removed and dried.

Silanization was performed as described previously [29,30]. Briefly, the samples were sonicated for 5 min in acetone and three times in distilled water. Subsequently, they were soaked for 6 h in 150 ml ethanol (96% vol., VWR) solution, where either 70 μL of APTES (99%, Sigma-Aldrich) or 70 mg of Q-APTES were dissolved [23]. The samples were then dried 1 h at 100 °C, sonicated for 5 min in ethanol, and finally dried again for 1 h at 100 °C.

All the treated samples were stored in multi-well plates in a desiccator.

2.2. Proteins

Three proteins were adsorbed onto the BG surfaces: fibronectin (fn), chimeric avidin (ChiAvd), and streptavidin (StrAvd). Fibronectin is a relatively large (monomer ~ 260 kDa) multi-domain protein that dimerizes via C-terminal disulfides. Fibronectin is highly soluble but fibril formation can be induced, leading to insoluble protein assemblies [31]. Chicken avidin and its bacterial cousin streptavidin are homotetrameric proteins with high affinity for biotin. This property could be exploited in successive studies to further functionalize materials via biotinylated agents, such as enzymes or growth factors [32], in which an ultrastable non-glycosylated recombinant variant of chicken avidin was used, termed ChiAvd [32]. Chimeric avidin and streptavidin are similar in size (~60 kDa) and oligomeric state, but differ in terms of surface charge; streptavidin is negatively charged (pI ~ 5) and ChiAvd positively charged (pI ~10). Fig. 1 shows the structures of the proteins used in this study.

2.2.1. Protein extraction

Proteins were extracted and purified from different sources.

Fn was extracted from human plasma preparations (octaplas). The full protocol was described in [33]. Briefly, 200 ml of Octaplas were warmed up to 37 °C inside a thermal bath, 2 mM phenylmethylsulfonyl fluoride (PMSF) and 10 mM ethylenediamine tetra-acetic acid (EDTA) were added. The solution obtained was centrifuged at 10′000 g for 15 min and purified using gelatin affinity chromatography (Gelatin-Sepharose 4 B; GE Healthcare) at a flow rate of 1–5 ml/min. Fn was eluted with phosphate-buffered saline (PBS) containing 3 M urea and dialyzed in PBS. Sodium dodecyl sulfate-polyacrylamide gel electrophoresis (SDS-PAGE) was performed to confirm the degree of purity. The purified fn was stored at −80 °C.

ChiAvd was recombinantly expressed in *Escherichia coli* (*E. coli*) and purified using affinity chromatography [34]. Briefly, *E. coli* single colonies were inoculated into lysogeny broth (LB) medium with the appropriate antibiotics, and the preculture was incubated for 6 h at 37 °C (200 rpm). The preculture was then placed in a fermentation medium (R2-medium). The R2-medium was prepared by first dissolving 2 g $(NH_4)_2HPO_4$, 6.75 g KH_2PO_4, 0.85 g citric acid and 2 g yeast extract in 1 L of ultrapure water, autoclaving the solution and successively adding 0.2 μm-filtered solutions of 1.4 ml MgSO4 (0.5 g/ml), 20 ml glucose (0.5 g/ml) and 5 ml trace metals. The composition of the trace metal 200x stock solution is shown in Table 2. Fermentation, lasting 24 h, was implemented in a Labfors Infors 3 fermentor (Infors HT, Bottmingen, Switzerland) at 28 °C, maintaining the oxygen level (pO_2 = 30%) and the pH (6.8) constant by continuous pH monitoring and eventual buffering with 15% NH_3 solution.

The antifoam agent Struktol J 647 (Schill + Seilacher, Hamburg, Germany) was added to prevent foam formation, and the feeding liquid was progressively added to the culture while maintaining the desired oxygen level. After 12 h, 1 mM isopropyl-β-D-1-thiogalactopyranoside (IPTG) was added and the temperature was decreased to 25 °C. Finally, the cells were collected by centrifugation and ChiAvd was purified with 2-iminobiotin-SepharoseTM 4 Fast Flow (Affiland, Liège, Belgium) from *E. coli* lysate. Analogous to fn preparation, SDS-PAGE was performed to confirm the degree of purity, and the protein was stored at −80 °C.

StrAvd, a recombinantly expressed protein, was obtained from Thermo Fisher Scientific (catalog number:21125).

All the proteins studied here (fn, ChiAvd, StrAvd) were labeled with the fluorophore Alexa Fluor 488-NHS ester (Succinimidyl Ester, Thermo Fisher Scientific) and detected by confocal fluorescence microscopy, once adsorbed by the BGs. The dye was dissolved in dimethyl-sulfoxide (DMSO) to obtain a solution with a final concentration of 10 mg/ml (15.5 mM). The dissolved dye was added to the protein solution (5–10 mg/ml protein in 0.1–0.2 M sodium bicarbonate buffer pH 8.3) while gently stirring and incubated at RT for 1 h with continuous stirring. To separate the labeled-protein solution and the unreacted fluorophore, extensive dialysis was performed with 50 mM Na-phosphate and 100 mM NaCl (pH = 7) using a 10 kDa cut-off membrane. The solutions obtained with labeled proteins are referred to as 488-fn, 488-ChiAvd, and 488-StrAvd, respectively.

After the extraction and labeling, the labeled protein solutions were aliquoted and stored at −20 °C.

2.2.2. Degree of labeling (DOL)

The DOL of the protein solutions, defined as the concentration of the fluorophore divided by the concentration of the protein of interest, was determined using UV–Vis spectroscopy (NanoDrop One, UV–Vis spectrometer, Thermo Scientific), which can assess the concentration of the grafted fluorophore and, consequently, of the protein of interest. A 2 μL drop of each solution (488-fn, 488-ChiAvd, and 488-StrAvd) was placed on the sensor using a micropipette. The absorbance values corresponding to wavelengths of 280 and 495 nm were measured. Finally, the DOL was calculated by applying Lambert–Beer law [35]. The resulting DOL values were 7.46, 1.65 and 0.91 labels per protein monomer for 488-fn, 488-ChiAvd and 488-StrAvd, respectively. These corresponded to protein concentrations of 4.55, 7.68 and 7.51 mg/ml, respectively.

2.2.3. Protein adsorption on BGs

Protein concentration on BGs, labeled (488-fn, 488-ChiAvd, 488-StrAvd) and non-labeled (fn, ChiAvd, StrAvd), was set to 15 μg/ml by dilution with PBS [20,21]. Protein adsorption was conducted in triplicate as follows. The BG substrates (untreated and pre-treated) were placed in a multi-well plate, and a 200 μL drop of 15 μg/ml protein

Table 2
Composition of the trace metal 200x stock solution for R2-medium preparation.

$FeSO_4 \cdot 7\ H_2O$	10 g
$CaCl_2 \cdot 2\ H_2O$	2 g
$CuSO_4 \cdot 5\ H_2O$	1 g
$ZnSO_4 \cdot 7\ H_2O$	2.5 g
$(NH_4)_6Mo_7O_{24} \cdot 4\ H_2O$	0.1 g
$Na_2B_4O_7 \cdot 10\ H_2O$	0.23 g
HCl 37%	415 ml
Ultrapure H_2O	to 1000 ml

solution (labeled or non-labeled) was deposited on the surface of each sample. Two negative controls were prepared by depositing either a 200 μL drop of PBS or a 200 μL drop of non-labeled protein on the BG surfaces. A coverslip (Precision cover glasses thickness No. 1.5H, Marienfeld Superior), on which a 200 μL-drop of the labeled protein was deposited, was used as a control. All the samples were incubated for 1 h at 37 °C. The samples were then mounted on a glass-bottom multi-well plate (SensoPlate™, 24-well plates, VWR) with a drop of a liquid mountant (ProLong™ Gold Antifade Mountant, Thermo Fisher Scientific). The samples were then gently positioned on the multi-well plates, with the surface of interest in contact with the bottom of the well to interface with the mountant. The samples were left to dry at RT overnight, covered with aluminum foil to protect them from light sources, and then analyzed by fluorescence confocal microscopy the next day.

2.3. Fluorescence confocal microscopy

Confocal microscopy (LSM800 GaAsP-Pmt1, Zeiss) was used to assess the degree of adsorption of labeled proteins on the materials. The laser settings were adjusted so that the autofluorescence from the substrate and the non-labeled proteins (negative control) were set close to zero and then subtracted from the images during analysis. Images were obtained using a Plan-Apochromat 63x/1.40 Oil DIC M27 objective lens. The channel imposed was relative to that of the dye (Alexa Fluor 488-NHS). The pinhole was set as 3.60 AU/156 μm. Experiments were performed in triplicate. Three randomly selected areas (1024 × 1024 pixels) were imaged on each surface of interest. All images were acquired and extracted using ZEN Blue 2.3 software (Zeiss) with the same settings.

Images were processed using an algorithm in MATLAB R2020a. The total fluorescence intensities were extracted from each image and averaged. The intensities recorded at the surface of the pretreated glasses were normalized to the intensity of the corresponding protein-coated bare glasses, and the untreated BG intensity was set to a value of 1. Normalization was performed to assess the increase or decrease in protein adsorption compared to the untreated surface.

2.4. Protein cluster analysis

To investigate the protein distributions on the surface of the substrates as a function of the pretreatment and to quantify the protein aggregation on the surfaces, an analysis of the protein clusters was performed as in [20], using the software CellAging [36]. After automatic segmentation followed by manual corrections, the number of clusters and their fluorescence were extracted using CellAging. An example of the results of the cluster segmentation is shown in Fig. 2.

The average pixel fluorescence intensities of the clusters, referred to as fluorescence per cluster, were obtained by summing the fluorescence of the clusters relative to their area and then dividing that by the number of clusters. To highlight the effects on protein adsorption as a function of pre-treatment, each parameter was normalized for each BG composition, using the value obtained for the untreated control sample (bare).

3. Results and discussion

The surfaces of the BG samples (S53P4, B25, SCNB, and PhGlass) were analyzed after labeled protein adsorption (488-fn, 488-ChiAvd, and 488-StrAvd) using fluorescence confocal microscopy. The calculation of the degree of labeling was fundamental for estimating the amount of adsorbed proteins on the surfaces and qualitatively evaluating their spatial distribution. The laser intensities were adjusted so that no significant autofluorescence was detected from the substrates in any of the pretreatments.

The adsorption of 488-fn and 488-ChiAvd was successful for all the substrates. Each substrate (composition and treatments) presented a different affinity for the proteins because the fluorescence intensities and surface distributions differed (Figs. 3 and 4). No fluorescence was detected after 488-StrAvd adsorption, suggesting that 488-StrAvd was not adsorbed onto any of the substrates. Previous studies have reported an almost null surface charge (slightly negative) characterizing streptavidin at physiological pH, which could explain the absent or negligible interactions with the substrates [37,38]. Therefore, we focused on 488-fn and 488-ChiAvd.

The mean fluorescence intensities for each glass composition, treatment, and both proteins are presented in Fig. 5.

Bioactive glass S53P4 is FDA-approved and commercially available. S53P4 is suitable for regeneration of critical bone defects [39]. This glass is osteostimulative and can prevent osteomyelitis to some extent [39,40]. The authors have already published the impact of silanization on surfaces washed under acidic, neutral, or basic conditions on fibronectin adsorption. Fibronectin had better adsorption on surfaces washed under neutral conditions and further silanized compared to the untreated condition [20]. A subsequent study indicated that when seeded with fibroblasts, S53P4 coated with fibronectin increased the cell attachment and proliferation on the biomaterial surface [21]. In this study, we assessed the impact of surface treatments on the adsorption abilities of fibronectin and chimeric avidin. As in [23,41], immersion in TRIS led to the precipitation of sporadic hydroxyapatite nodules but mainly to the formation of a hydrated layer at the glass surface. Immersion in SBF led to the precipitation of a thick hydroxyapatite/hydroxycarbonate apatite (HA/HCA) layer [4,23,42]. The net surface charge was less negative upon immersion in both TRIS and SBF (from −47.88 mV for the bare sample, to −12.12 mV and −5.64 mV for the TRIS and SBF treated samples, respectively) [23]. Soaking S53P4 in TRIS/SBF preserved the same affinity as 488-fn, as observed by the comparable fluorescence intensity (Fig. 5(A)) with the tendency of the protein to aggregate into

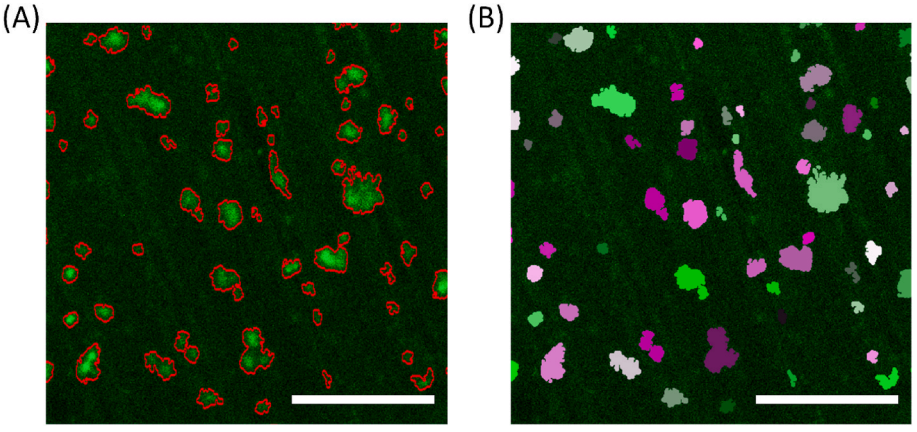

Fig. 2. Example of protein clusters' segmentation following the 488-fn adsorption on the surface of PhGlass APTES. (A) Results of automatic cluster segmentation. The borders detected of the identified protein clusters are represented by the red lines. (B) Areas of each cluster identified in (A) were colored to visually determine the quality of the segmentation. These were used for potential manual corrections, when needed. The scalebars represent 20 μm. (For interpretation of the references to color in this figure legend, the reader is referred to the Web version of this article).

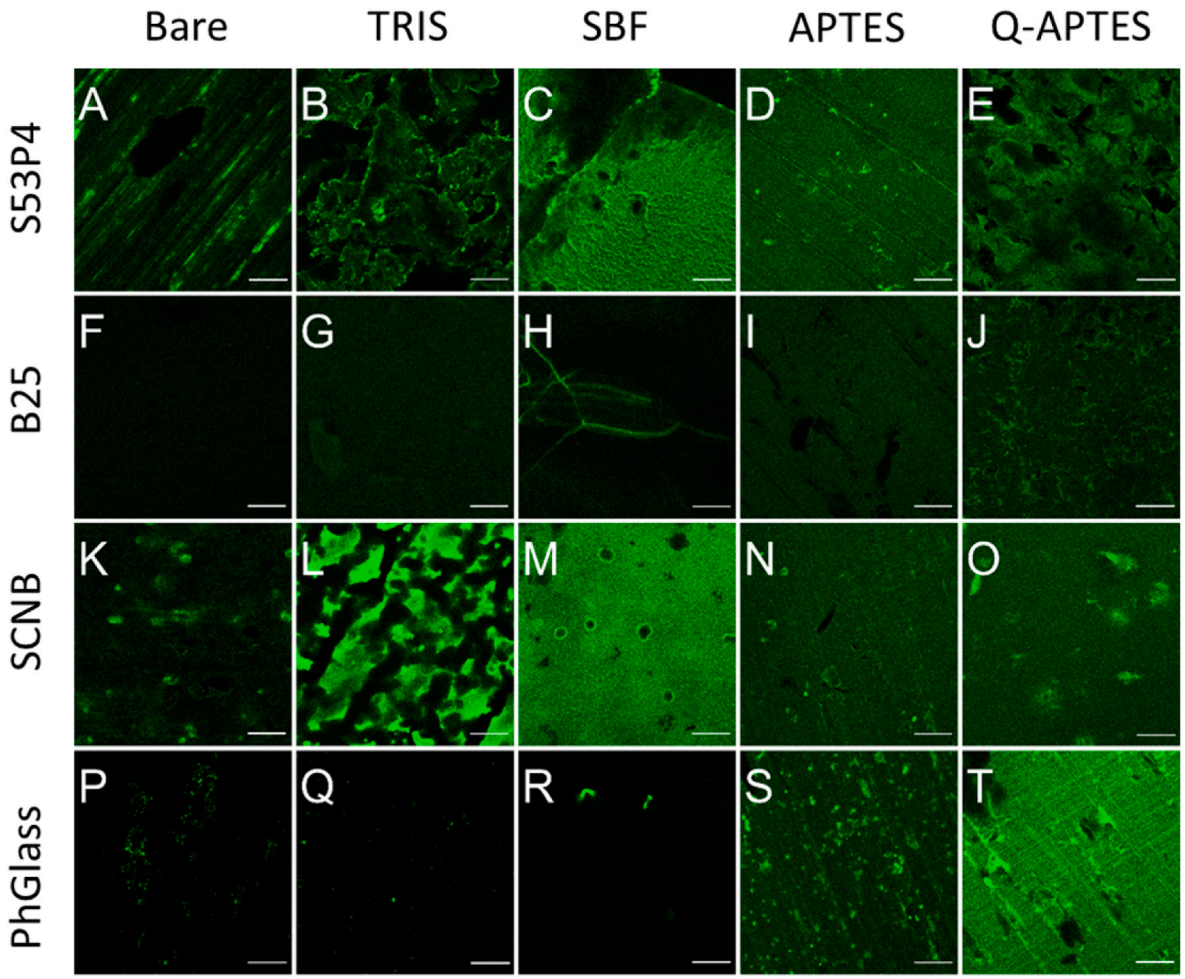

Fig. 3. Representative images showing 488-fn adsorption on the surface of: (A) bare, (B) TRIS, (C) SBF, (D) APTES and (E) Q-APTES S53P4; (F) bare, (G) TRIS, (H) SBF, (I) APTES and (J) Q-APTES B25; (K) bare, (L) TRIS, (M) SBF, (N) APTES and (O) Q-APTES SCNB; (P) bare, (Q) TRIS, (R) SBF, (S) APTES and (T) Q-APTES PhGlass. The scalebars are 10 μm.

macro-clusters, creating a less uniform surface distribution (Fig. 3 (B–C)). Specifically, after immersion in TRIS, S53P4 exhibited a slightly higher fluorescence intensity and a different surface distribution than the untreated surface. On TRIS-treated S53P4, 488-fn appears to adhere to the precipitated phase organized in partially detached layers, whose higher intensity on the edges suggests their tendency to create back-folded structures. Conversely, after immersion in SBF, despite the higher tendency of 488-fn to adhere to the surface, non-uniform protein adsorption occurred, as shown by the larger error bar (Fig. 5(A)). This may be due to the higher roughness (as shown previously in [23]) induced by the precipitation of HA/HCA, which exposes a larger interaction area owing to the higher surface-to-volume ratio [23,43]. Concerning silanization, S53P4 showed an increase in affinity with 488-fn after APTES grafting, given the higher fluorescence intensity (Fig. 3(D) and 5(A)), as well as a more uniform and homogeneous surface coverage, while preserving the same affinity in the case of Q-APTES (Fig. 3(E) and 5(A)). In the case of 488-ChiAvd, no significant improvement in its adsorption on S53P4 was observed after pretreatment. The difference between APTES and Q-APTES may lie in the ratio between the neutral and protonated amino groups, leading to the modulation of surface charge/hydrophobicity. Indeed, APTES functionalization led to a greater density of protonated amino groups than functionalization with Q-APTES [23]. This is consistent with the preferential binding of fibronectin to positively charged surfaces [44]. Conversely, chimeric avidin shows lower affinity to the treated surfaces (Fig. 4(A-E), 5(B)) due to the preferential binding of chimeric avidin to negatively charged surfaces [45]. However, APTES- and Q-APTES--grafted S53P4 uniformly covered the surface.

The B25 composition is based on S53P4, where 25 wt % of the SiO_2 content is substituted with B_2O_3, yielding borosilicate glass [4,46]. It is noteworthy that B25 bioactive glass has a lower hydrolytic resistance than S53P4 and promotes the conversion of the glass into HA/HCA at a higher rate. For instance, we previously observed that B25 immersed in TRIS promoted the precipitation of a thick HA/HCA reactive layer on the glass surface [4,23]. Therefore, it can be assumed that the surface chemical natures of the B25 glass immersed in TRIS and SBF are identical. Fibronectin adsorption revealed no significant difference between the bare sample and the samples immersed in TRIS or SBF (Fig. 3(G-H) and 5(C)). This is related to the high density of hydroxyl groups in both bare glass and hydroxyapatite [23,47]. However, an increase in fibronectin affinity was observed in the silanized samples (Fig. 3(I-J) and 5 (C)). The surface coverage was more uniform on APTES-treated B25. In contrast, Q-APTES induced only slight protein aggregation. These aggregations could have been caused by fibronectin unfolding when adsorbed on the surface. This promotes polymerization, and consequently, fibrillogenesis [48]. As mentioned, this can be due to the preferential binding of fibronectin to positively charged amino groups [23]. The fluorescent signal of 488-ChiAvd adsorbed on silanized B25 was comparable to that on the untreated substrate, although the distribution was less homogeneous (Fig. 4(F-J), 5(D)). Neither TRIS nor SBF caused significant changes in surface distribution, but a small decrease in 488-ChiAvd surface binding affinity was suggested by the lower

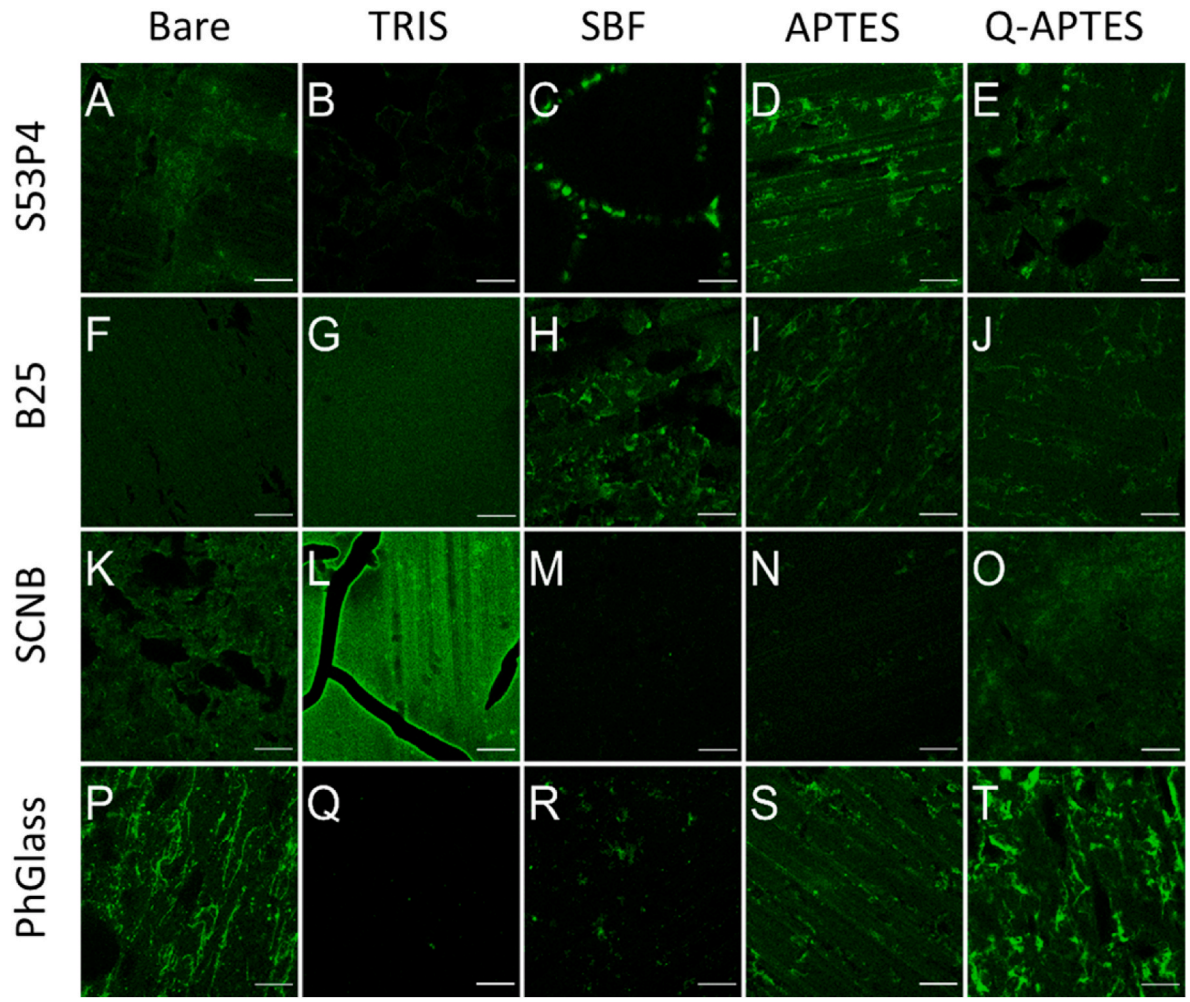

Fig. 4. Representative images showing 488-ChiAvd adsorption on the surface of: (A) bare, (B) TRIS, (C) SBF, (D) APTES and (E) Q-APTES S53P4; (F) bare, (G) TRIS, (H) SBF, (I) APTES and (J) Q-APTES B25; (K) bare, (L) TRIS, (M) SBF, (N) APTES and (O) Q-APTES SCNB; (P) bare, (Q) TRIS, (R) SBF, (S) APTES and (T) Q-APTES PhGlass. The scalebars are 10 μm.

fluorescent signal (0.52 and 0.48 times the fluorescence of the bare substrate after soaking in TRIS and SBF, respectively).

SCNB bioactive glass is more stable than S53P4 because its initial composition does not contain phosphorus. Therefore, while immersion in SBF promotes the precipitation of HA, immersion in TRIS only promotes the formation of a hydrated layer [23,49]. SCNB showed a significantly increased affinity to 488-fn after each of the pre-treatments (TRIS, SBF, APTES, Q-APTES) compared to the untreated surface (Fig. 3 (K–O), 5(E)). Soaking the substrate either in TRIS or SBF increased the fluorescent signal ~5 times more than that on the untreated substrate. Despite the comparable fluorescence between TRIS- and SBF-treated surfaces, the surface distribution of 488-fn differed: TRIS-treated SCNB presented a clustered coverage with some areas devoid of fluorescence signal, whereas a more homogeneously covered surface was observed on the SBF-treated substrate (Fig. 3(L-M)). This can be explained by the different chemistries of the two surfaces. The hydrated TRIS-treated SCNB is characterized by a smoother surface than the SBF-treated substrate which, due to the HA/HCA precipitation, exposes a higher area for the protein-biomaterial interactions, similar to S53P4 [23,43,49]. Silanization induced a higher fluorescent signal (~2 times higher than that on the bare substrate) and more uniform coverage of the surface, especially on APTES-treated SCNB. Q-APTES also induced a few 488-fn macroaggregations on a more homogeneous protein layer. Similar to what was observed for Q-APTES-treated B25, surface-induced fibronectin fibrillogenesis may occur under these conditions [48]. In the case of 488-ChiAvd, TRIS significantly increased the affinity between SCNB and 488-ChiAvd, inducing a 2 times higher fluorescent signal (Fig. 5(F)). The protein distribution was uniform on the grains of the precipitated reactive layer, whereas no protein was detected in the gaps between them (Fig. 4(L)). In contrast, SBF and APTES drastically decreased the affinity to 488-ChiAvd (Fig. 4(M) and 5(F)), likely owing to the lower absolute value of the zeta potential [45]. The affinity between the protein and SCNB decreased drastically after silanization with APTES. Conversely, it was preserved in the case of Q-APTES, through which analog fluorescence was maintained, as well as a similar surface distribution, compared to the bare substrate (Fig. 4(K–O), 5(F)).

Phosphate glasses are bioresorbable and degrade congruently. Immersion in TRIS and SBF promoted the formation of a reactive layer, which was assigned to dicalcium phosphate dihydrate [23]. Furthermore, based on previous studies, alkaline and alkaline earth depletion of the top surface can be expected [50]. Another metaphosphate glass was surface functionalized using APTES. Surface functionalization increased the fibronectin affinity and promoted cell adhesion, whereas the cells could not attach to the material without a fibronectin coating [20,21]. In accordance with previous studies on metaphosphate glasses [20,21], we found no affinity for 488-fn on a bare substrate (Fig. 3(P), 5(G)). This is maintained on the TRIS- and SBF-soaked samples, as observed by the comparable fluorescent signals close to zero (Fig. 5(G)) and agrees with the characteristic congruent dissolution and ion depletion [50]. However, silanization induced a significant improvement in 488-fn

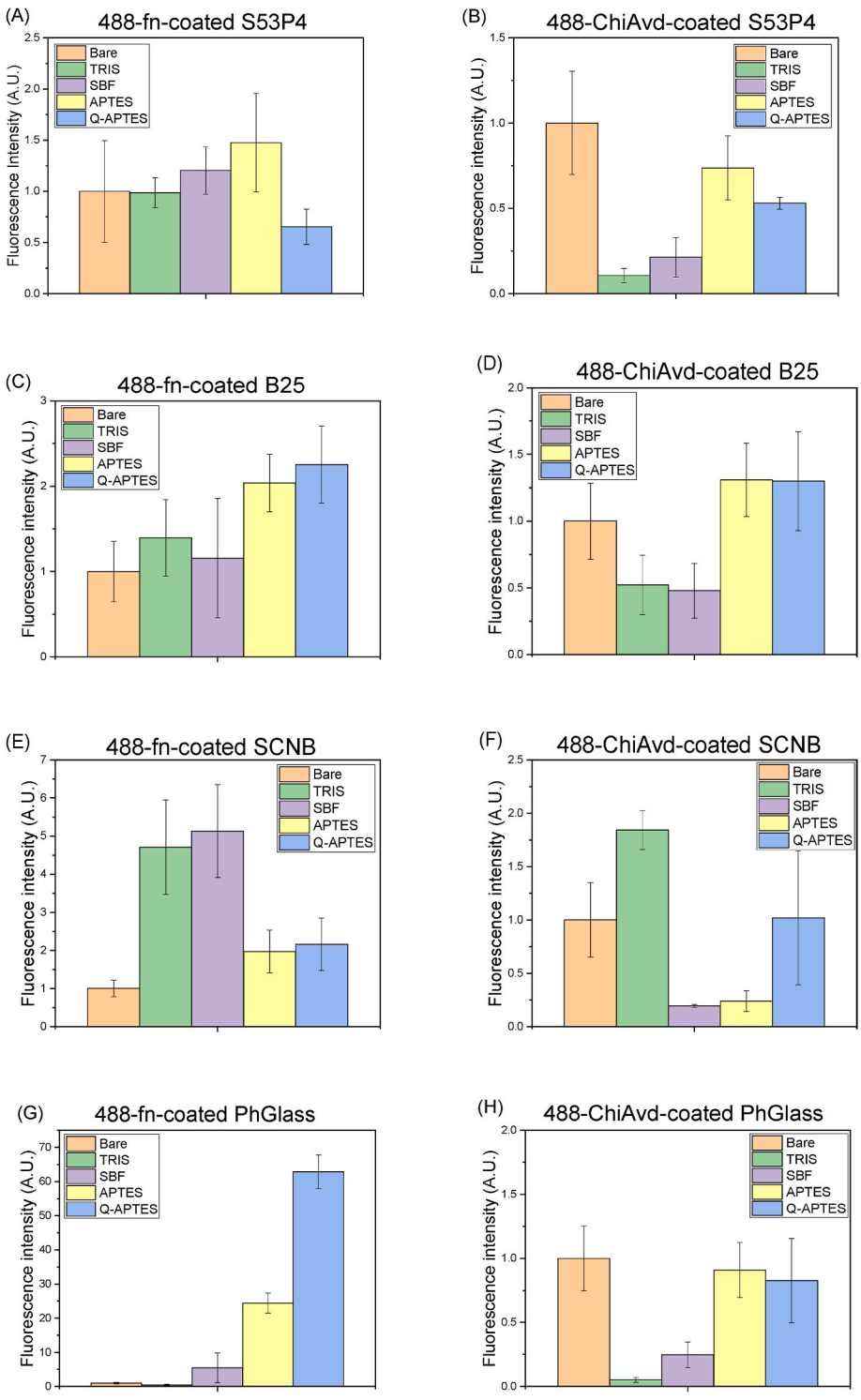

Fig. 5. Normalized average relative fluorescence intensity of the different BGs after 488-fn/488-ChiAvd adsorption. Intensities were normalized with setting the untreated BG intensity to value of 1. Data from the surfaces of (A) 488-fn-coated and (B) 488-ChiAvd-coated S53P4, (C) 488-fn-coated and (D) 488-ChiAvd-coated B25, (E) 488-fn-coated and (F) 488-ChiAvd-coated SCNB, (G) 488-fn-coated and (H) 488-ChiAvd-coated PhGlass. Graphs are showing triplicate samples with standard deviation. Vertical error bars represent the standard deviation from the triplicates.

adsorption on this substrate (Fig. 3(S-T), 5(G)), as previously reported [20], where grafting APTES on PhGlass led to a 20 times stronger fluorescent signal than that on the untreated substrate, whereas after grafting with Q-APTES, the signal was 80 times higher (Fig. 5(G)). The surface distribution of 488-fn was quite homogeneous on the APTES-treated surface, whereas the coverage was even more uniform in the case of grafted Q-APTES (Fig. 3(S-T)). 488-ChiAvd presented a higher affinity to bare PhGlass compared to 488-fn (Figs. 4 and 5). A similar preference was preserved after silanization, with comparable fluorescent signals and comparable distributions (Fig. 4(S-T), 5(H)). The coverage was slightly more uniform in the case of APTES and with the presence of some macro-aggregations in the case of Q-APTES (Fig. 4 (S-T)).

For a deeper, quantitative analysis of proteins adsorption and their distribution over the surfaces of interest, a semi-automated image analysis was performed on the clusters in the confocal microscopy images. The relative numbers of clusters (no. clusters), and the fluorescence intensity per cluster was evaluated and compared as a function of the pretreatment of each BG composition, as in [20]. The values were normalized to the respective bare substrates to compare the effect of the

pre-treatments on protein adsorption. The results were reported for 488-fn (Fig. 6) and 488-ChiAvd (Fig. 7).

Silicate and borosilicate BGs (S53P4, B25, SCNB) generally indicated a decrease in the number of 488-fn clusters and an increase in the fluorescence intensity (total and per cluster, as shown in Figs. 5 and 6 (B), respectively) after each pre-treatment. This suggests a higher and more uniform adsorption of the protein after the pretreatment of the substrates. The decrease in the number of 488-fn clusters is evident after soaking the surface in TRIS/SBF, whereas in the case of silanization (APTES/Q-APTES), the values are closer to those in the untreated surfaces (Fig. 6(A)). This can be explained by the different roughness/surface topography of these substrates (presented in [23]): silanized silicate/borosilicate BGs have a surface roughness comparable to that of untreated BGs, while the reactive layer and the phase precipitated after soaking in TRIS/SBF contributed to an increase in the contact surface area. The higher area available for interactions with proteins, as well as the presence of microcavities on these surfaces, may contribute to a more homogeneous 488-fn distribution on TRIS- and SBF-soaked substrates [23]. Indeed, it is expected that the fibronectin size of 120–160 nm [51] and that of HA/HCA nodules of 50–60 nm [52], leading to microcavities smaller than the size of the protein when the HA/HCA layer is fully formed. In such cases, the surface roughness stabilizes through the interaction with the microcavities and the protein coating against folding and fibrillogenesis, thereby decreasing their ability to reassemble on the surface [53]. Furthermore, there is a similar trend between silanized silicate/borosilicate glasses, for which the fluorescence per cluster was twice as high as that on bare substrates (Fig. 6(B)). This agrees with previous studies [20]. Concerning soaking in TRIS/SBF, a different behavior was observed: the fluorescence per cluster of silicate glasses (S53P4, SCNB) was four times more intense, whereas the borosilicate glass (B25) maintained statistically comparable values before and after the treatment (Fig. 6(B)). Overall, the fluorescence per cluster measured for each surface correlated well with the total fluorescence (Fig. S1). This confirms the generally uniform coverage of the surfaces of silicate/borosilicate BGs by 488-fn. The only exceptions include TRIS-, SBF-, and Q-APTES-treated S53P4, for which the increase in fluorescence per cluster was higher than the increase in total fluorescence, which is in accordance with the less homogeneous 488-fn distribution on these surfaces, as previously observed by qualitative evaluation (Fig. 3(A-E)).

Concerning 488-ChiAvd (Fig. 7), only a weak correlation was observed between the number of clusters and the fluorescence per cluster on the silicate and borosilicate glasses. We also did not observe any specific trend characterizing the analyzed surfaces for 488-fn. This may be related to the fact that avidins do not form a polymer layer like fibronectin does. Therefore, it is impossible to induce local polymerization via surface chemistry [48,54]. Silicate glasses (S53P4, SCNB) show analogous numbers of clusters after each pretreatment, which are statistically comparable to the value on the untreated surface (Fig. 7(A)). Conversely, borosilicate glass (B25) presented a strong increase in the number of clusters after soaking in TRIS and after silanization (APTES/Q-APTES), which was approximately seven times higher than that on the bare substrate (Fig. 7(A)). This is consistent with the less homogeneous 488-ChiAvd coverage on these substrates, as qualitatively observed in Fig. 4(F-J). In contrast to 488-fn, the fluorescence emitted by 488-ChiAvd from the silicate and borosilicate glasses showed the same trend, with no significant difference between the total and per-cluster values (Fig. 5(B, D, F), 7(B)). This can be interpreted as an overall stronger adsorption and more uniform surface coverage [20]. Generally, silanized silicate and borosilicate BGs (APTES/Q-APTES) presented similar fluorescence compared to untreated substrates, suggesting no significant difference in 488-ChiAvd adsorption after silanization. Soaking in TRIS and SBF decreased the affinity between 488-ChiAvd and the substrates, given the lower fluorescence and comparable/lower number of clusters (Fig. 7). This can be explained by the more homogeneous distribution of Si–OH groups, compared to the bare substrates, owing to the high hydration induced by the treatments. The only exception is TRIS-treated SCNB, whose fluorescence (total and per cluster) nearly doubled (Fig. 5(F) and 7(B)), probably because of the absence of phosphorus in its bulk composition and the consequent different surface chemistry [49]. Indeed, phosphorus-free BGs, as reported in previous studies, showed limited bioactivity in environments that do not contain any phosphorus (such as TRIS) because of the absence of this element, which is fundamental for HA/HCA precipitation [23,49].

The phosphate glass (PhGlass), as observed by confocal microscopy, did not present any measurable affinity to 488-fn when untreated and after soaking in TRIS/SBF (Fig. 6). The number of clusters decreased after soaking PhGlass in TRIS/SBF, while the fluorescence (both total and per cluster) showed no statistical difference from that of the bare substrate (Fig. 5(G), 6(B)). Instead, a significant increase in the number of clusters and fluorescence per cluster was observed after silanization, especially with Q-APTES (Fig. 6). Furthermore, the greater increase in the total fluorescence (~20 and ~80 times higher after grafting APTES and Q-APTES, respectively, than in untreated substrates) and in the fluorescence per cluster (approximately 4 and 9 times, respectively) confirmed the highly uniform coverage of the surface by the protein with few aggregations (Fig. 5(G), 6(A)). These results are consistent with those of a previous study that investigated 488-fn adsorption on three different compositions of phosphate glasses [20].

In contrast, the number of 488-ChiAvd clusters on PhGlass did not indicate any statistical difference from the bare surface after any pretreatment (Fig. 7(A)). The fluorescence per cluster showed a trend analogous to the total fluorescence, suggesting that the fluorescence was primarily emitted by the clustered protein, consistent with what was qualitatively observed in Fig. 4(P-T). The lower fluorescence per cluster after soaking PhGlass in TRIS/SBF (nearly half the intensity compared to the initial one) suggests a lower affinity between 488-ChiAvd and the treated substrate, probably due to congruent dissolution and ion depletion [23,50,55,56]. The fluorescence (total and per cluster) did not

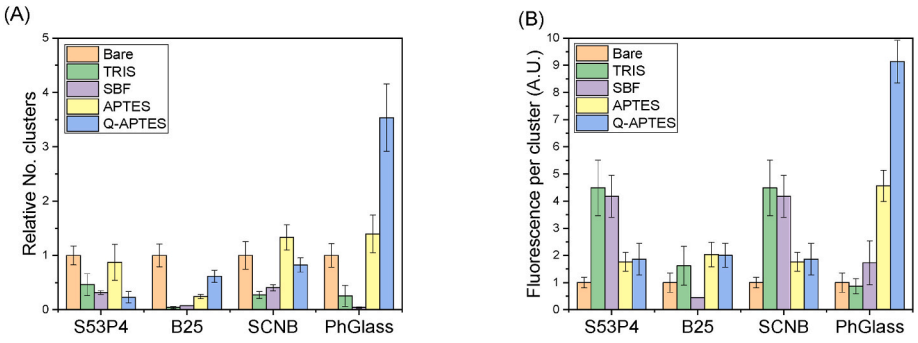

Fig. 6. 488-fn cluster analysis on bare (untreated) and pre-treated substrates: (A) relative number of clusters (No. clusters) and (B) relative fluorescence per cluster. Average of three independent tests. Vertical error bars are the standard deviation from the triplicates.

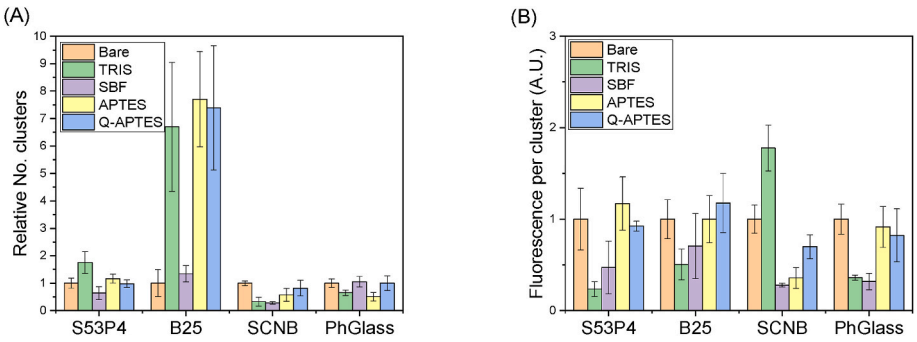

Fig. 7. 488-ChiAvd cluster analysis on bare (untreated) and pre-treated substrates: (A) relative number of clusters (No. clusters), (B) relative fluorescence per cluster. Average of three independent tests. Vertical error bars are the standard deviation from the triplicates.

indicate significant differences after silanization (APTES/Q-APTES), confirming the maintenance of the same affinity and surface distribution on silanized PhGlass, as observed qualitatively in Fig. 4(P-T).

4. Conclusions

We compared the adsorption of model proteins on different surface-treated BG compositions and correlated it with the physicochemical properties of the substrates. Four BG compositions (two silicates, one borosilicate, and one phosphate glass) and four surface modifications (soaking in TRIS or SBF, grafting of APTES, or Q-APTES) were considered. Untreated surfaces were used as the controls. Fibronectin, chimeric avidin, and streptavidin were considered model proteins and labeled for detection and quantification by confocal microscopy in fluorescence modality. Fibronectin and chimeric avidin were successfully adsorbed onto the substrates, with affinity and surface distribution differing from the physics and chemistry of each surface. Streptavidin was not affine to any substrate, potentially because of the charge repulsion. Further image processing was performed to quantitatively determine the amount and surface distribution of fibronectin and the chimeric avidin.

Stronger and more homogeneous adsorption of fibronectin on all BGs was observed after silanization, particularly on the phosphate glass (Fig. 3). Uniform coverage was also obtained by soaking the silicate and borosilicate glasses in TRIS/SBF (Fig. 3). This suggests that surface chemistry is critical in the affinity between the proteins and substrates, while roughness mainly affects the homogeneity of the coverage.

The adsorption of chimeric avidin was less substrate-dependent than fibronectin, indicating increased adsorption and higher homogeneity after silanization, as well as a lower amount of adsorbed protein after soaking in TRIS/SBF when compared to the untreated surface (Fig. 4).

Overall, it was observed that the TRIS- and SBF-treated BGs presented higher variability in the response to protein adsorption. This was hypothesized to be related to the different glass compositions, roughnesses, and surface chemistries, leading to the precipitation of different ceramic phases (HA/HCA and calcium phosphate dihydrate) at the interface. Their different chemical structures and reactivities highly impact protein adsorption kinetics, making the density, surface distribution, and conformation of the adsorbed proteins difficult to predict. In contrast, grafting APTES or Q-APTES on the glass surfaces led to homogeneous functionalization with molecules favoring uniform interactions with the targeted proteins. This promoted a controlled and homogeneous protein coating (confocal microscopy). It is hypothesized that silanization of substrates leads to a more predictable protein conformation. In the near future, we plan to compare protein adsorption in static and dynamic conditions and study the impact of surface treatments on protein secondary structures.

Declaration of competing interest

The authors declare that they have no known competing financial interests or personal relationships that could have appeared to influence the work reported in this paper.

Acknowledgements

This project was funded by the European Union's Horizon 2020 Research and Innovation Program under the Marie Skłodowska-Curie grant agreement [No 860462 (PREMUROSA)]. The authors also acknowledge the Academy of Finland, Sigrid Juselius Foundation, and Cancer Foundation of Finland for their financial support. Biocenter Finland (BF) and the Tampere Imaging Facility (TIF) are acknowledged for their infrastructure support.

Appendix A. Supplementary data

Supplementary data to this article can be found online at https://doi.org/10.1016/j.ceramint.2022.12.157.

References

[1] L.L. Hench, R.J. Splinter, W.C. Allen, T.K. Greenlee Jr., Bonding mechanisms at the interface of ceramic prosthetic materials, J. Biomed. Mater. Res. 5 (6) (1971) 117–141, https://doi.org/10.1002/jbm.820050611.
[2] L.L. Hench, Bioglass: 10 milestones from concept to commerce, J. Non-Cryst. Solids 423 (2016) 2–8, https://doi.org/10.1016/j.jnoncrysol.2014.12.038.
[3] M. Schumacher, P. Habibovic, S. van Rijt, Mesoporous bioactive glass composition effects on degradation and bioactivity, Bioact. Mater. 6 (2021) 1921–1931, https://doi.org/10.1016/j.bioactmat.2020.12.007.
[4] S. Ferraris, A. Nommeots-Nomm, S. Spriano, E. Vernè, J. Massera, Surface reactivity and silanization ability of borosilicate and Mg-Sr-based bioactive glasses, Appl. Surf. Sci. 475 (2019) 43–55, https://doi.org/10.1016/j.apsusc.2018.12.218.
[5] B. Thavornyutikarn, B. Feltis, P.F.A. Wright, T.W. Turney, Effect of pre-treatment of crystallized bioactive glass with cell culture media on structure, degradability, and biocompatibility, Mater. Sci. Eng. C 97 (2019) 188–197, https://doi.org/10.1016/j.msec.2018.12.034.
[6] M. Rabe, D. Verdes, S. Seeger, Understanding protein adsorption phenomena at solid surfaces, Adv. Colloid Interface Sci. 162 (2011) 87–106, https://doi.org/10.1016/j.cis.2010.12.007.
[7] I. Notingher, A.R. Boccaccini, J. Jones, V. Maquet, L.L. Hench, Application of Raman microspectroscopy to the characterisation of bioactive materials, Mater. Char. 49 (2003) 255–260, https://doi.org/10.1016/S1044-5803(03)00029-9.
[8] K. Zheng, M. Kapp, A.R. Boccaccini, Protein interactions with bioactive glass surfaces: a review, Appl. Mater. Today 15 (2019) 350–371, https://doi.org/10.1016/j.apmt.2019.02.003.
[9] U. Filipović, R.G. Dahmane, S. Ghannouchi, A. Zore, K. Bohinc, Bacterial adhesion on orthopedic implants, Adv. Colloid Interface Sci. 283 (2020), 102228, https://doi.org/10.1016/j.cis.2020.102228.
[10] P. Jurczak, J. Witkowska, S. Rodziewicz-Motowidło, S. Lach, Proteins, peptides and peptidomimetics as active agents in implant surface functionalization, Adv. Colloid Interface Sci. 276 (2020), 102083, https://doi.org/10.1016/j.cis.2019.102083.
[11] U. Filipović, R.G. Dahmane, S. Ghannouchi, A. Zore, K. Bohinc, Bacterial adhesion on orthopedic implants, Adv. Colloid Interface Sci. 283 (2020), 102228, https://doi.org/10.1016/j.cis.2020.102228.
[12] L.L. Hench, J.K. West, Biological applications of bioactive glasses, Life Chem. Rep. 13 (1996) 187.
[13] N. Marín-Pareja, E. Salvagni, J. Guillem-Marti, C. Aparicio, M.P. Ginebra, Collagen-functionalised titanium surfaces for biological sealing of dental implants: effect of immobilisation process on fibroblasts response, Colloids Surf. B Biointerfaces 122 (2014) 601–610, https://doi.org/10.1016/j.colsurfb.2014.07.038.

[14] A. Baranowski, A. Klein, U. Ritz, A. Ackermann, J. Anthonissen, K.B. Kaufmann, C. Brendel, H. Götz, P.M. Rommens, A. Hofmann, Surface functionalization of orthopedic titanium implants with bone sialoproitein, PLoS One 11 (4) (2016), e0153978, https://doi.org/10.1371/journal.pone.0153978.

[15] E.B. Bae, J.H. Yoo, S.I. Jeong, M.S. Kim, Y.M. Lim, J.J. Ahn, J.J. Lee, S.H. Lee, H. J. Kim, J.B. Huh, Effect of titanium implants coated with radiation crosslinked collagen on stability and osseointegration in rat tibia, Materials 11 (12) (2018) 2520, https://doi.org/10.3390/ma11122520.

[16] N.T. Truc, H.H. Minh, L.L. Khan, V.M. Thuy, V.V. Toi, T.V. Man, H.C.N. Nam, T. N. Quyen, N.T. Hiep, Modification of type I collagen on TiO2 surface using electrochemical deposition, Surf. Coating. Technol. 344 (2018) 664–672, https://doi.org/10.1016/j.surfcoat.2018.03.038.

[17] Y.C. Chang, K.N. Ho, S.W. Feng, H.M. Huang, C.H. Chang, C.T. Lin, N.C. Teng, Y. H. Pan, W.J. Chang, Fibronectin-grafted titanium dental implants: an in vivo study, BioMed Res. Int. 2016 (2016), 2414809, https://doi.org/10.1155/2016/2414809.

[18] V. Wagner, A.R. Boccaccini, S. Virtanen, Protein-adsorption and Ca-phosphate formation on chitosan-bioactive glass composite coatings, Appl. Surf. Sci. 416 (2017) 454–460, https://doi.org/10.1016/j.apsusc.2017.04.051.

[19] C. Gruian, A. Vulpoi, H.-J. Steinhoff, S. Simon, Structural changes of methemoglobin after adsorption on bioactive glass, as a function of surface functionalization and salt concentration, J. Mol. Struct. 1015 (2012) 20–26, https://doi.org/10.1016/j.molstruc.2012.01.045.

[20] N.B. Hyunh, C. Santos Dias Palma, R. Rahikainen, A. Mishra, L. Azizi, E. Vernè, S. Ferraris, V.P. Hytönen, A. Sanches Ribeiro, J. Massera, Surface modification of bioresorbable phosphate glasses for controlled protein adsorption, ACS Biomater. Sci. Eng. 7 (9) (2021) 4483–4493, https://doi.org/10.1021/acsbiomaterials.1c00735.

[21] L. Azizi, P. Turkki, N. Huynh, J.M. Massera, V.P. Hytönen, Surface modification of bioactive glass promotes cell attachment and spreading, ACS Omega 6 (35) (2021) 22635–22642, https://doi.org/10.1021/acsomega.1c02669.

[22] A. Cerqueira, F. Romero-Gavilán, I. García-Arnáez, C. Martinez-Ramos, S. Ozturand, I. Iloro, M. Azkargorta, F. Elortza, R. Izquierdo, M. Gurruchaga, I. Goñi, J. Suaya, Bioactive zinc-doped sol-gel coating modulates protein adsorption patterns and in vitro cell responses, Mater. Sci. Eng. C 121 (2021), 111839, https://doi.org/10.1016/j.msec.2020.111839.

[23] V.A. Gobbo, V.S. Parihar, M. Prato, M. Kellomäki, E. Vernè, S.M. Spriano, J. Massera, Surface modification of silicate, borosilicate and phosphate bioactive glasses to improve/control protein adsorption: part I, Ceramic. Int. 49 (1) (2023) 1261–1275, https://doi.org/10.1016/j.ceramint.2022.09.105.

[24] M. Wilchek, E.A. Bayer, The avidin-biotin complex in bioanalytical applications, Anal. Biochem. 171 (1) (1988) 1–32, https://doi.org/10.1016/0003-2697(88)90120-0.

[25] O.H. Laitinen, H.R. Nordlund, V.P. Hytönen, M.S. Kulomaa, Brave new (strept) avidins in biotechnology, Trends Biotechnol. 25 (6) (2007) 268–277, https://doi.org/10.1016/j.tibtech.2007.04.001.

[26] A. Jain, K. Cheng, The principles and applications of avidin-based nanoparticles in drug delivery and diagnosis, J. Contr. Release 245 (2017) 27–40, https://doi.org/10.1016/j.jconrel.2016.11.016.

[27] V. Ettelt, K. Ekat, P.W. Kämmerer, B. Kreikemeyer, M. Epple, M. Veith, Streptavidin-coated surfaces suppress bacterial colonization by inhibiting non-specific protein adsorption, J. Biomed. Mater. Res. 106 (3) (2017) 758–768, https://doi.org/10.1002/jbm.a.36276.

[28] T. Kokubo, K. Hata, T. Nakamura, T. Yamamuro, Apatite formation on ceramics, metals and polymers induced by CaO SiO2 based glass in a simulated body fluid, Bioceramics (1991) 113–120, https://doi.org/10.1016/B978-0-7506-0269-3.50020-7. Proceedings of the 4th International Symposium on Ceramics in Medicine London, UK, September.

[29] J. Massera, A. Mishra, S. Guastella, S. Ferraris, E. Vernè, Surface functionalization of phosphate-based bioactive glasses with 3-aminopropyltriethoxysilane (APTS), Biomedical Glasses 2 (2016) 51–62, https://doi.org/10.1515/bglass-2016-0007.

[30] A. Deraine, M.T. Rebelo Calejo, R. Agniel, M. Kellomäki, E. Pauthe, M. Boissière, J. Massera, Polymer-based honeycomb films on bioactive glass: toward a biphasic material for bone tissue engineering applications, ACS Appl. Mater. Interfaces 13 (25) (2021), 29984, https://doi.org/10.1021/acsami.1c03759.

[31] G. Baneyx, L. Baugh, V. Vogel, Fibronectin extension and unfolding within cell matrix fibrils controlled by cytoskeletal tension, Proc. Natl. Acad. Sci. USA 99 (8) (2002) 5139–5143, https://doi.org/10.1073/pnas.072650799.

[32] V.P. Hytönen, J.A.E. Määttä, T.K.M. Nyholm, O. Livnah, Y. Eisenberg-Domovich, D. Hyre, H.R. Nordlind, J. Hörnä, E.A. Niskanen, T. Paldanius, T. Kulomaa, E. K. Porkka, P.S. Stayton, O.H. Laitinen, M.S. Kulomaa, Design and construction of highly stable, protease-resistant chimeric avidins, J. Biol. Chem. 280 (11) (2005) 10228–10233, https://doi.org/10.1074/jbc.M414196200.

[33] E. Ruosalhti, E.G. Hayman, M. Pierschbacher, E. Engvall, Fibronectin: purification, immunochemical properties, and biological activities, Methods Enzymol. 82 (1982) 803–831, https://doi.org/10.1016/0076-6879(82)82103-4.

[34] V.P. Hytönen, O.H. Laitinen, T.T. Airenne, H. Kidron, N.J. Meltola, E.J. Porkka, J. Hörhä, T. Paldanius, J.A.E. Määttä, H.R. Nerlund, M.S. Johnson, T.A. Salminen, K.J. Airenne, S. Ylä-Herttuala, M.S. Kulomaa, Efficient production of active chicken avidin using a bacterial signal peptide in Escherichia coli, Biochem. J. 384 (Pt 2) (2004) 384–385, https://doi.org/10.1042/BJ20041114.

[35] J. Leppiniemi, J.A.E. Määttä, H. Hammaren, M. Soikkeli, M. Laitaoja, J. Jänis, M. S. Kulomaa, V.P. Hytönen, Bifunctional avidin with covalently modifiable ligand binding site, PLoS One 6 (1) (2011), e16576, https://doi.org/10.1371/journal.pone.0016576.

[36] A. Häkkinen, A.-B. Muthukrishnan, A. Mora, J.M. Fonseca, A.S. Ribeiro, CellAging: a tool to study segregation and partitioning in division in cell lineages of Escherichia coli, Bioinformatics 29 (2013) 1708–1709, https://doi.org/10.1093/bioinformatics/btt194.

[37] M.D. Savage, G. Mattson, S. Desai, G.M. Nielander, S. Morgensen, E.J. Conklin, Avidin-Biotin Chemistry, A Handbook, second ed., Rockford, Pierce, 1994.

[38] L. Almonte, E. Lopez-Elvira, A.M. Barò, Surface-charge differentiation of streptavidin and avidin by atomic force microscopy-force spectroscopy, ChemPhysChem 15 (13) (2014) 2768–2773, https://doi.org/10.1002/cphc.201402234.

[39] N.C. Lindfors, I. Koski, J.T. Heikkilä, K. Mattila, A.J. Aho, A prospective randomized 14-year follow-up study of bioactive glass and autogenous bone as bone graft substitutes in benign bone tumors, J. Biomed. Mater. Res. B Appl. Biomater. 94B (1) (2010) 157–164, https://doi.org/10.1002/jbm.b.31636.

[40] M. Gonzalez Moreno, M.E. Butini, E.M. Maiolo, L. Sessa, A. Trampuz, Antimicrobial activity of bioactive glass S53P4 against representative microorganisms causing osteomyelitis – real-time assessment by isothermal microcalorimetry, Colloids Surf. B Biointerfaces 189 (2020), 110853, https://doi.org/10.1016/j.colsurfb.2020.110853.

[41] S.V. Sirkiä, M. Nakamura, S. Qudsia, M. Siekkinen, J.-H. Smått, J. Peltonen, T. J. Heino, L. Hupa, P.K. Vallittu, Structural and elemental characterization of glass and ceramic particles for bone surgery, Dent. Mater. 37 (9) (2021) 1350–1357, https://doi.org/10.1016/j.dental.2021.06.004.

[42] Ö.H. Andersson, I. Kangasniemi, Calcium phosphate formation at the surface of bioactive glass in vitro, J. Biomed. Mater. Res. 25 (8) (1991) 1019–1030, https://doi.org/10.1002/jbm.820250808.

[43] S. Ferraris, S. Yamaguchi, N. Barbani, M. Cazzola, C. Cristallini, M. Miola, E. Vernè, S. Spriano, Bioactive materials: in vitro investigation of different mechanisms of hydroxyapatite precipitation, Acta Biomater. 102 (2020) 468–480, https://doi.org/10.1016/j.actbio.2019.11.024.

[44] E. Liamas, K. Kubiak-Ossowska, R.A. Black, O.R.T. Thomas, Z.J. Zhang, P. A. Mulheran, Adsorption of fibronectin fragment on surfaces using fully atomistic molecular dynamics simulations, Int. J. Mol. Sci. 19 (11) (2018) 3321, https://doi.org/10.3390/ijms19113321.

[45] T.A. Riihimäki, S. Kukkurainen, S. Varjonen, J. Hörhä, T.K.M. Nyholm, M. S. Kulomaa, V.P. Hytönen, Construction of chimeric dual-chain avidin by tandem fusion of the related avidins, PLoS One 6 (5) (2011), e20535, https://doi.org/10.1371/journal.pone.0020535.

[46] M. Ojansivu, A. Mishra, S. Vanhatupa, M. Juntunen, A. Larionova, J. Massera, S. Miettinen, The effect of S53P4-based borosilicate glasses and glass dissolution products on the osteogenic commitment of human adipose stem cells, PLoS One 13 (8) (2018), e0202740, https://doi.org/10.1371/journal.pone.0202740.

[47] J. Brzezińska-Miecznik, P. Jeleń, K. Haberko, W. Mozgawa, M. Sitarz, The effect of NaOH and KOH treatment on the behavior of CO32- and OH- groups in natural origin hydroxyapatite, Ceramics Interantional 43 (15) (2017) 12540–12545, https://doi.org/10.1016/j.ceramint.2017.06.127.

[48] M. Mitsi, S. Handschin, I. Gerber, R. Schwartländer, E. Klotzsch, R. Wepf, V. Vogel, The ultrastructure of fibronectin fibers pulled from a protein monolayer at the air-liquid interface and the mechanism of the sheet-to-fiber transition, Biomaterials 36 (2015) 66–79, https://doi.org/10.1016/j.biomaterials.2014.08.012.

[49] J.R. Jones, O. Tsigkou, E.E. Coates, M.M. Stevens, J.M. Polak, L.L. Hench, Extracellular matrix formation and mineralization on a phosphate-free porous bioactive glass scaffold using primary human osteoblast (HOB) cells, Biomaterials 28 (9) (2007) 1653–1663, https://doi.org/10.1016/j.biomaterials.2006.11.022.

[50] J. Massera, A. Mishra, S. Guastella, S. Ferraris, E. Verné, Surface functionalization of phosphate-based bioactive glasses with 3-aminopropyltriethoxysilane (APTS), Biomedical Glasses 2 (1) (2016) 51–62, https://doi.org/10.1515/bglass-2016-0007.

[51] H.P. Erickson, N. Carrell, J. McDonagh, Fibronectin molecule visualized in electron microscopy: a long, thin, flexible strand, J. Cell Biol. 91 (3 Pt 1) (1981) 673–678, https://doi.org/10.1083/jcb.91.3.673.

[52] M. Rabiei, A. Palevicius, A. Monshi, S. Nasiri, A. Vilkauskas, G. Janusas, Comparing methods for calculating nano crystals size of natural hydroxyapatite, using X-ray diffraction 10 (9) (2020) 1627, https://doi.org/10.3390/nano10091627.

[53] M. Pehueroles, C. Aparicio, M. Bosio, E. Engel, F.J. Gil, J.A. Planell, G. Altankov, Spatial organization of osteoblast fibronectin matrix on titanium surfaces: effects of roughness, chemical heterogeneity and surface energy, Acta Biomater. 6 (1) (2010) 291–301, https://doi.org/10.1016/j.actbio.2009.07.030.

[54] D.M. Taylor, H. Morgan, C. D'Silva, Behavior of avidin and avidin/bisbiotin polymers at the air-water interface, J. Colloid Interface Sci. 144 (1) (1991) 53–62, https://doi.org/10.1016/0021-9797(91)90237-3.

[55] J. Massera, K. Bourhis, L. Petit, M. Couzi, L. Hupa, M. Hupa, J.J. Videau, T. Cardinal, Effect of the glass composition on the chemical durability of zinc-phosphate-based glasses in aqueous solutions, J. Phys. Chem. Solid. 74 (2013) 121–127, https://doi.org/10.1016/j.jpcs.2012.08.010.

[56] N. Jmal, J. Bouaziz, Synthesis, characterization and bioactivity of a calcium-phosphate glass-ceramics obtained by the sol-gel processing method, Mater. Sci. Eng. C 71 (2017) 279–288, https://doi.org/10.1016/j.msec.2016.09.058.